Temperature-dependent Lowering of Coercive Field in 300 nm Sputtered Ferroelectric $Al_{0.70}Sc_{0.30}N$

Ved Gund[1], Benyamin Davaji[1], Hyunjea Lee[1], Mohammad Javad Asadi[1], Joseph Casamento[2], Huili Grace Xing[1,2,3], Debdeep Jena[1,2,3], and Amit Lal[1]

[1]Electrical and Computer Engineering
Cornell University
Ithaca, NY, USA

[2]Materials Science and Engineering
Cornell University
Ithaca, NY, USA

[3]Kavli Institute at Cornell
Cornell University
Ithaca, NY, USA

2021 IEEE International Symposium on Applications of Ferroelectrics (ISAF) | 978-1-6654-0444-0/20/$31.00 ©2021 IEEE | DOI: 10.1109/ISAF51943.2021.9477328

Abstract — **This paper reports the temperature-dependent ferroelectric properties of sputtered ferroelectric $Al_{0.70}Sc_{0.30}N$. The coercive field is experimentally demonstrated to decrease by 1.5 MV/cm in 300 nm films in the temperature range of 20–193 ^{0}C, corresponding to an average linear coefficient of decrease of 8.8 kV/^{0}C. In the same range, the remnant polarization varies by 23.5% between 90-114 µC/cm^2 without a significant drop-off at higher temperatures. Thermally cycling the chip between room temperature and the highest achievable temperature of 193 ^{0}C shows a reversible tuning of the coercive field, paving the path towards on-chip ovenization-based control of ferroelectric properties. The dielectric breakdown under AC and DC testing are driven by filamentary and thermally driven breakdown processes respectively. These breakdown processes suggest the potential for high frequency operation of sputtered $Al_{0.70}Sc_{0.30}N$ as a ferroelectric thin film at elevated temperatures with low leakage.**

Keywords – ***Ferroelectricity, Ferroelectric Thin Films, Aluminum Scandium Nitride, Coercive Field, Piezoelectric***

I. INTRODUCTION

Thin-film aluminum nitride (AlN) has been enabling to the RF filter technology for the past two decades, owing to the high Figure-of-Merit $Q^*k_t^2$ for AlN film bulk acoustic resonator (FBAR) device [1]–[3]. To increase the electromechanical coupling coefficient (k_t^2) for larger fractional bandwidths of RF filters, scandium-doped AlN ($Al_{1-x}Sc_xN$) has been proposed which can increase the piezoelectric coupling by as much as a factor of 4 for x = 0.4, with experimental demonstrations of RF resonators confirming these predictions [4], [5].

Recently, Fichtner et al. have shown that highly doped $Al_{1-x}Sc_xN$ with $0.27 < x < 0.43$ is ferroelectric with a box-like polarization vs electric field (PE) loop and remnant polarization P_r of 80-100 µC/cm^2, which is attractive for applications in reconfigurable filters, memory devices and analog computation [6]. Ferroelectricity has since been demonstrated in highly-doped $Al_{1-x}Sc_xN$ films with thickness 500 nm down to 20 nm, and with Sc-doping as low as 10% [7]–[9]. A major challenge with the device integration of $Al_{1-x}Sc_xN$ is the relatively high coercive field E_C in the 4-7 MV/cm range for ferroelectric switching, which necessitates large on-chip voltages. Efforts to engineer a lower E_C have focused on tuning film stress, temperature control via in situ heating and introduction of alternative dopants such as boron [10]–[12].

Established ferroelectric materials such as hafnium zirconium oxide and lead zirconate titanate (PZT) have been previously shown to achieve lowered coercive fields at high temperatures due to a reduced energy barrier for switching [13], [14]. Preliminary reports on the temperature-dependence of ferroelectricity in $Al_{0.70}Sc_{0.30}N$ have shown a similar reduction in E_C [11], but have not identified the impact of thermal cycling on ferroelectricity as well as dielectric breakdown properties. This paper systematically studies the effect of temperature on the ferroelectric properties of $Al_{0.70}Sc_{0.30}N$ and reports on the lowered values of E_C at temperatures up to 200 ^{0}C without a substantial change in P_r. The paper also explores the temperature-dependence of the dielectric breakdown field E_{BD} in the ferroelectric material with both AC and DC IV testing.

II. FABRICATION AND EXPERIMENTAL SETUP

A. $Al_{0.70}Sc_{0.30}N$ Deposition and Material Characterization

300 nm ferroelectric $Al_{0.70}Sc_{0.30}N$ thin film was deposited by reactive co-sputtering on a 200 nm molybdenum (Mo) continuous bottom electrode in an OEM Endeavor PVD cluster tool that has a dual-target S-gun magnetron [15]. Both, the $Al_{0.70}Sc_{0.30}N$ and the Mo, were templated on 30 nm AlN seed layers as templates to promote a c-axis oriented growth in the $Al_{0.70}Sc_{0.30}N$. A high degree of crystallinity was confirmed in the $Al_{0.70}Sc_{0.30}N$ film with an X-ray diffraction (XRD) Omega-scan that had a full width half maximum (FWHM) of 2.1^0 (Fig. 1A). 200 nm of aluminum was then deposited and patterned to form the top electrode for the ferroelectric capacitors.

B. Experimental Setup

Fig. 1B shows a schematic of the experimental setup used for temperature-dependent characterization of ferroelectric properties. An etch chemistry to pattern $Al_{0.70}Sc_{0.30}N$ was not available at the time of this report, so a "top electrode only" probing configuration was used. The input waveform was applied to a circular electrode of 40 µm diameter (probe 1) and the sense current was measured from a much larger electrode of 30 µm x 1800 µm (probe 2) which was shorted to the bottom Mo via dielectric breakdown of the $Al_{0.70}Sc_{0.30}N$ under it. The effective capacitor in this configuration is the vertical capacitor between the 40 µm electrode and continuous bottom electrode, because of the disparity in the size of the areas. A Thorlabs HT19R ceramic heater (rated for a maximum power and temperature of 24W and 400 ^{0}C respectively) was used for in situ temperature control and a TH100PT resistance temperature device (RTD) was bonded with thermal epoxy to monitor and characterize the stage temperature as a function of input power to the heater (Fig. 1C). The chip temperature T vs. heater power P_{in} has a linear fit with the dependence given by:

$$T = 14.4P_{in} + 23.7 \quad (1)$$

The maximum temperature achieved was 193 ^{0}C, which is below the maximum rating due to conductive losses to the stage used for mounting the device, which has a high thermal mass. The $Al_{0.70}Sc_{0.30}N$ capacitor was connected in a Sawyer-

978-1-6654-0444-0/21/$31.00 ©2021 IEEE
Authorized licensed use limited to: Cornell University Library. Downloaded on April 24,2022 at 05:53:08 UTC from IEEE Xplore. Restrictions apply.

Tower circuit [16], driven by an arbitrary waveform generator, to generate the positive-up-negative-down (PUND) waveforms (Fig. 1D) with equal rise, fall, and wait times for continuous wave (CW) operation. The signal was amplified with an EPA-102 piezo amplifier with a maximum output voltage of ±200V over a 250 kHz bandwidth. The polarization current on the P and N cycles was extracted by subtracting the leakage currents on the U and D cycles respectively, to calculate the switching current density as a function of E-field and extract the PE loop.

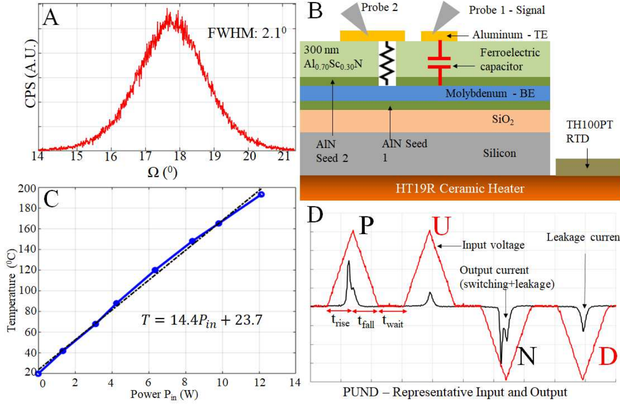

Figure 1: A). XRD Omega-scan of $Al_{0.70}Sc_{0.30}N$ with FWHM of 2.1^0. B). Experimental setup for temperature-dependent characterization of ferroelectricity with top electrode only probing. C). Calibration of ceramic heater and chip temperature T (in ^{0}C) as a function of input power P_{in} (in W). D). Representative applied voltages for positive-up-negative-down (PUND) cycles, and sense output current, which has contributions from both the switching charge and the leakage current.

III. EXPERIMENTAL RESULTS

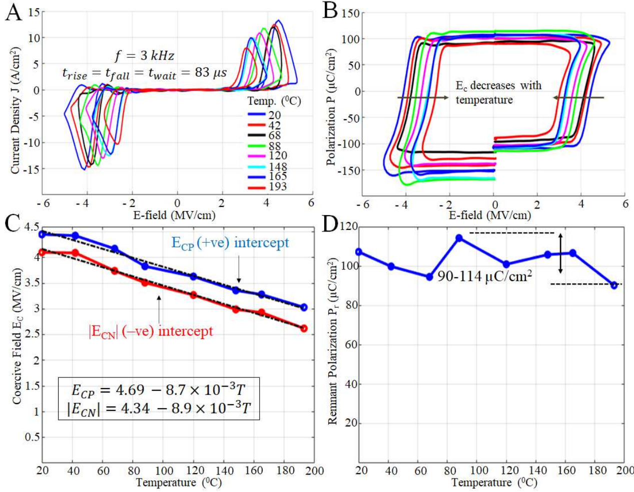

Figure 2: A). Switching current density J vs. E-field at 3 kHz switching pulse frequency for temperatures from 20–193 ^{0}C. B). PE loops show a monotonic decrease in the coercive field E_C at successively higher temperatures. C). Linear regression fits for the positive and negative intercepts (E_{CP} and E_{CN}) of the coercive field vs temperature with coefficients of –8.7 and –8.9 kV/^{0}C. D). Remnant polarization P_r vs. temperature does not show significant variation and has a non-monotonic trend due to contributions from leakage currents.

A. Temperature-dependence of E_C and P_r

Fig. 2A plots switching current density J versus input E-field with a PUND input and pulse frequency of 3 kHz ($t_{rise} = t_{fall} = t_{wait}$ = 83 μs). Both, the peak value of J and the E-field at which the peak is observed, monotonically decrease at successively higher temperatures due to the reduced coercive field and the corresponding decrease in the switching current for the same polarization charge. The reduction in E_C is confirmed with PE loops (Fig. 2B) for both the positive and negative pulses. Fig. 2C shows a linear regression fit for the magnitudes of the positive and negative intercepts of coercive field (E_{CP} and E_{CN}) in MV/cm vs. temperature as:

$$E_{CP} = 4.69 - 8.7 \times 10^{-3} T \quad (2)$$

$$|E_{CN}| = 4.34 - 8.9 \times 10^{-3} T \quad (3)$$

The average value of the coefficient for E-field scaling with temperature is –8.8 kV/^{0}C, in the range of temperatures tested. P_r varies between 90-114 μC/cm^2 and has a non-monotonic trend due to contributions from the leakage current in the measurements (Fig. 2D).

B. Temperature Cycling

To study the reversibility of ferroelectric properties under temperature cycling, the wafer was cycled between room temperature (20 ^{0}C) and the highest achievable temperature with the setup (193 ^{0}C). Fig. 3A shows the switching current density vs E-field for 3 such cycles. The wafer was allowed to thermally equilibrate at each temperature and the J vs E plot and PE loops were obtained after stabilization for > 1000 cycles under CW PUND operation. There is a clear split between the room temperature and high temperature operation with repeatable behavior at each temperature. The PE loops (Fig. 3B) show that E_C can be reversibly tuned by up to 1.5 MV/cm in this range of temperatures without a substantial change in P_r, thus demonstrating the capability of reversible on-chip control of coercive field in $Al_{0.70}Sc_{0.30}N$ by in situ heating. Both E_{CP} and E_{CN} can be tuned in this manner (Fig. 3C). P_r is also observed to have a variation of ~ 15 μC/cm^2 with two distinguishable levels at 20 ^{0}C and 193 ^{0}C but the split in values is reduced due to contributions from the leakage current (Fig. 3D).

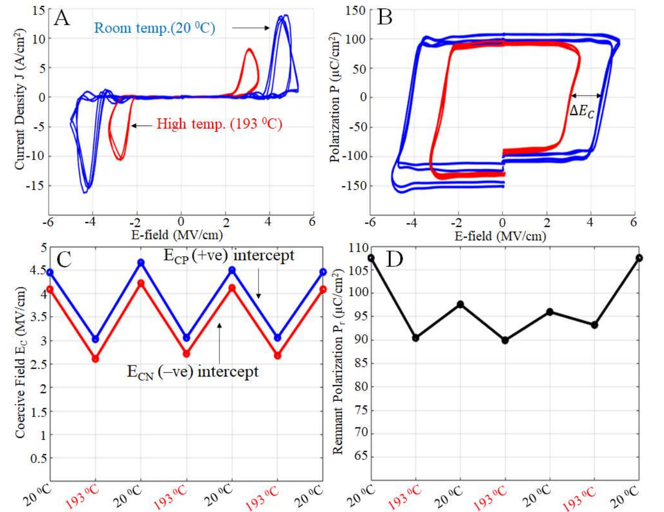

Figure 3: A). Overlay of switching current density J vs. E-field for 3 temperature cycles between 20 ^{0}C and 193 ^{0}C. B). PE loops showing a reversibility in coercive field tuning between the two temperatures. C). Reversible cycling of E_{CP} and E_{CN} with 1.5 MV/cm tuning in the temperature range D). P_r shows distinct levels at the two temperatures but contributions from leakage current confound the measurements.

C. $Al_{0.70}Sc_{0.30}N$ Breakdown Field

The dielectric breakdown field E_{BD} in $Al_{0.70}Sc_{0.30}N$ was studied with continuous wave AC PUND E-field switching

Authorized licensed use limited to: Cornell University Library. Downloaded on April 24,2022 at 05:53:08 UTC from IEEE Xplore. Restrictions apply.

as a function of temperature, with a different electrode used for each measurement due to the destructive nature of the breakdown. The breakdown is identified as a shorting of the drive electrode to the bottom Mo. A typical post-breakdown resistance of < 20Ω was observed. Fig. 4A shows that E_{BD} is ~5 MV/cm from 20-120 ^{0}C and does not decrease with temperature, unlike E_C. In fact, E_{BD} marginally increases to 6.6 MV/cm at 160 ^{0}C. However, this breakdown is filamentary and chemical in nature, as indicated by the absence of visible damage to the ferroelectric capacitor or electrodes. A caveat in this measurement is that it does not fully quantify the leakage current, so a DC IV test was conducted to monitor leakage current vs input E-field for three different temperatures (Fig. 4B), which shows that the DC current density for a given E-field increases with temperature. Additionally, DC breakdown is a thermally driven process that leads to ablation of the metal electrode and produces an open circuit, unlike the AC measurement. This distinction between AC and DC breakdown could be potentially harnessed for high frequency ferroelectric switching at higher temperatures that can minimize damage to the ferroelectric and reduce the impact of leakage.

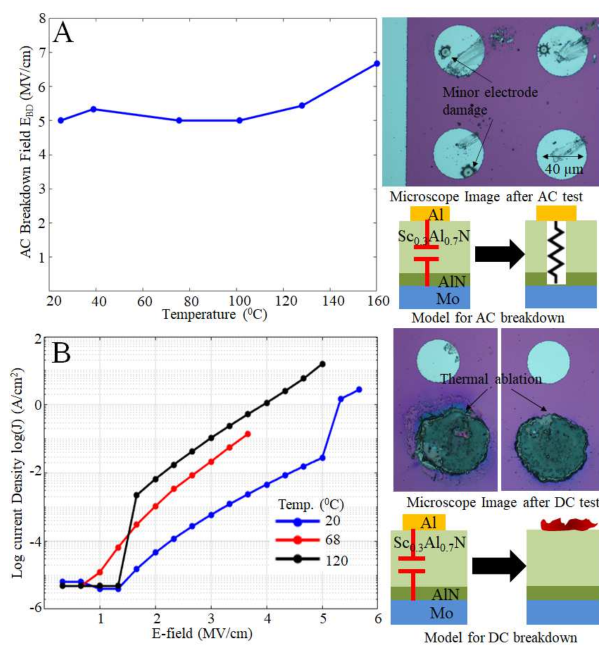

Figure 4: A). Dielectric breakdown field E_{BD} observed during continuous wave (CW) AC PUND switching. Microscope images of tested capacitors show minimal damage owing to the filamentary breakdown that shorts the top and bottom electrodes. B). DC I-V leakage current at three different temperatures showing increased leakage at higher temperatures. Microscopic images show thermal ablation of electrodes caused by destructive breakdown producing an open circuit.

CONCLUSIONS

The ferroelectric properties of 300 nm $Al_{0.70}Sc_{0.30}N$ were measured over the range of temperatures from 20-193 ^{0}C with a top electrode probing configuration. The films showed a monotonic reduction in coercive field from 4.3 MV/cm to 2.6 MV/cm with increasing temperatures, demonstrating a path towards low-voltage device operation. In the same range, the remnant polarization varied non-monotonically between 90-114 µC/cm^2 with variations due to leakage current contributions at higher temperatures. We have also demonstrated the reversible on-chip control of coercive field by cycling the chip between the lowest and highest temperatures. Distinct mechanisms of AC and DC breakdown in the samples indicate that high frequency high temperature ferroelectric operation of $Al_{0.70}Sc_{0.30}N$ can reduce the coercive field and leakage current while mitigating the chances of thermally induced breakdown in the film.

ACKNOWLEDGMENT

This work was performed in part at the Cornell NanoScale Facility (CNF), an NNCI member supported by NSF Grant NNCI-2025233 and made use of the Cornell Center for Materials Research (CCMR) Shared Facilities which are supported through the NSF MRSEC program (DMR-1719875). Funding was also provided by the DARPA TUFEN program, monitored by Dr. Ron Polcawich.

REFERENCES

[1] R. Ruby, P. Bradley, J. D. Larson, and Y. Oshmyansky, “PCS 1900 MHz duplexer using thin film bulk acoustic resonators (FBARs),” *Electron. Lett.*, vol. 35, no. 10, pp. 794–795, May 1999.

[2] R. Ruby, “A decade of FBAR success and what is needed for another successful decade,” in *Proceedings of the 2011 Symposium on Piezoelectricity, Acoustic Waves and Device Applications, SPAWDA 2011*, 2011, pp. 365–369.

[3] R. H. Olsson, J. G. Fleming, K. E. Wojciechowski, M. S. Baker, and M. R. Tuck, “Post-CMOS compatible aluminum nitride MEMS filters and resonant sensors,” in *Proceedings of the IEEE International Frequency Control Symposium and Exposition*, 2007, pp. 412–419.

[4] M. Akiyama, K. Kano, and A. Teshigahara, “Influence of growth temperature and scandium concentration on piezoelectric response of scandium aluminum nitride alloy thin films,” *Appl. Phys. Lett.*, vol. 95, no. 16, p. 162107, Oct. 2009.

[5] L. Colombo, A. Kochhar, C. Xu, G. Piazza, S. Mishin, and Y. Oshmyansky, “Investigation of 20% scandium-doped aluminum nitride films for MEMS laterally vibrating resonators,” Oct. 2017.

[6] S. Fichtner, N. Wolff, F. Lofink, L. Kienle, and B. Wagner, “AlScN: A III-V semiconductor based ferroelectric,” *J. Appl. Phys.*, vol. 125, no. 11, p. 114103, Mar. 2019.

[7] M. Pirro, B. Herrera, M. Assylbekova, G. Giribaldi, L. Colombo, and M. Rinaldi, “Characterization of Dielectric and Piezoelectric Properties of Ferroelectric AlScN Thin Films,” in *Proceedings of the IEEE International Conference on Micro Electro Mechanical Systems (MEMS)*, Jan. 2021, vol. 2021-Janua, pp. 646–649.

[8] D. Wang *et al.*, “Ferroelectric Switching in Sub-20 nm Aluminum Scandium Nitride Thin Films,” *IEEE Electron Device Lett.*, vol. 41, no. 12, pp. 1774–1777, Dec. 2020.

[9] S. Yasuoka *et al.*, “Effects of deposition conditions on the ferroelectric properties of (Al1- xSc x)N thin films,” *J. Appl. Phys.*, vol. 128, no. 11, p. 114103, Sep. 2020.

[10] D. Wang *et al.*, “Ferroelectric C-Axis Textured Aluminum Scandium Nitride Thin Films of 100 nm Thickness,” Jul. 2020.

[11] J. Wang, M. Park, S. Mertin, T. Pensala, F. Ayazi, and A. Ansari, “A Film Bulk Acoustic Resonator Based on Ferroelectric Aluminum Scandium Nitride Films,” *J. Microelectromechanical Syst.*, vol. 29, no. 5, pp. 741–747, Oct. 2020.

[12] J. Hayden *et al.*, “Ferroelectricity in boron-substituted aluminum nitride thin films,” *Phys. Rev. Mater.*, vol. 5, no. 4, p. 044412, Apr. 2021.

[13] J. Muller *et al.*, “Ferroelectric hafnium oxide: A CMOS-compatible and highly scalable approach to future ferroelectric memories,” 2013.

[14] X. Chen *et al.*, “Temperature dependence of ferroelectricity and domain switching behavior in Pb(Zr0·3Ti0.7)O3 ferroelectric thin films,” *Ceram. Int.*, vol. 45, no. 14, pp. 18030–18036, Oct. 2019.

[15] V. Gund *et al.*, “Towards Realizing the Low-Coercive Field Operation of Sputtered Ferroelectric ScxAl1-xN,” *TRANSDUCERS 2021- 21st Int. Conf. Solid-State Sensors, Actuators Microsystems*, in press.

[16] C. B. Sawyer and C. H. Tower, “Rochelle salt as a dielectric,” *Phys. Rev.*, vol. 35, no. 3, pp. 269–273, Feb. 1930.

Authorized licensed use limited to: Cornell University Library. Downloaded on April 24,2022 at 05:53:08 UTC from IEEE Xplore. Restrictions apply.